Journal of CO_2 Utilization 24 (2018) 164–173

Contents lists available at ScienceDirect

Journal of CO_2 Utilization

journal homepage: www.elsevier.com/locate/jcou

CO_2 sequestration by pH-swing mineral carbonation based on HCl/NH_4OH system using iron-rich lizardite 1T

Gretta Larisa Aurora Arce Ferrufino[a,c,d,*], Sayuri Okamoto[a], Jose Carlos Dos Santos[a], João Andrade de Carvalho Jr.[c], I. Avila[c], Carlos Manuel Romero Luna[b,d], Turibio Gomes Soares Neto[a]

[a] Combustion and Propulsion Associated Laboratory, Brazilian Space Research Institute (LCP/INPE), Brazil
[b] Production Engineering, Campus of Itapeva, São Paulo State University (UNESP), Brazil
[c] Combustion and Carbon Capture Laboratory, Energy Department, Campus of Guaratinguetá, São Paulo State University (LC3/DEN/UNESP), Brazil
[d] Advanced Materials and Nanotechnology Research Group, Faculty of Chemical and Metallurgical Engineering, Jose Faustino Sanchez Carrion National University (UNJFSC), Huacho, Lima, Peru

ARTICLE INFO

Keywords:
Mining waste
Lizardite 1T
pH-swing mineral carbonation
HCl/NH_4OH system
Carbonates
CO_2 sequestration

ABSTRACT

In pH-swing mineral carbonation, several acid/base systems has been investigated. Currently the main acid/base systems employed are HCl/NaOH and NH_4HSO_4/NH_4OH. However, the use of a HCl/NH_4OH system was not yet elucidated. This study proposes to evaluate the feasibility of a pH-swing mineral carbonation based on HCl/NH_4OH system at atmospheric pressure and moderate temperatures using mining waste from asbestos production from Goiás State, Brazil (S-GO) for two conditions (i.e. stoichiometric conditions (T2E) and acid excess (T2)). Results indicated that the Fe^{3+} content in S-GO acted as a catalyst, due to $FeCl_3$ hydrolysis in aqueous solutions. Thus, high Mg and Fe extraction efficiency (95 ± 2%), were achieved in the leaching stage for both conditions. The S_1 solid residue was mainly SiO_2 with 90 ± 1% purity content. In the purification stage 91.7 ± 1.9% of Fe_t were removed, however, a loss of Mg of 13.6 ± 2.3% was also detected. On the carbonation stage, high purity hydromagnesite was formed in T2E; this stage had a 85% efficiency, thus, 36.7% of CO_2 was fixed. On T2, excess H_2O and CO_2 promoted dypingite formation and reduced hydromagnesite formation. After carbonation, the formation of crystals was observed in the NH_4Cl aqueous solution at 25 °C, indicating NH_4Cl supersaturation. The results of mass balance indicate that 4 ton of mineral waste will be employed for each ton of captured CO_2, as well as 2.6 ton of HCl, and 4.5 ton of NH_4OH. However, 1.7 ton of SiO_2, 0.55 ton of iron oxides, and 2.7 ton of hydromagnesite could be produced.

1. Introduction

Sterile is a residue from a mining step related to asbestos production, normally disposed of in landfills. However, since it has low chrysotile contents, it is considered a hazardous waste and its disposal represents a challenge for environmental engineering and public health [1–5]. According to Valuoma et al. [5], Fedoročková et al. [6], and Gadikota et al. [1], carbon capture and storage by mineralization (CCSM) using asbestos-containing materials is a technology that would have several environmental benefits, since it can permanently alter the asbestos fiber structure in these materials, as well as sequester carbon dioxide (CO_2) in a safe and permanent manner, producing materials with high aggregated value in the market. This would avoid disposal issues normally associated to these mining wastes [7].

Among all CCSM methodologies, the pH-swing mineral carbonation is recently receiving more attention, since it presents a favorable kinetics. Besides this, it would allow obtainment of useful products and subproducts, which could be commercialized, reducing elevated costs associated to such processes [28–13]. Although many challenges have been overcome by employing the pH-swing mineral carbonation, there are other issues that still remain unsolved. The major hurdle is related to the high energy consumption, making it difficult to insert this technology at industrial scale [13].

Great part of the energy consumption is linked to acid and base recovery, mainly used for pH control. High leaching efficiency is associated to pH under 1 (for example, in the extraction of reactive elements such as Mg, Ca, and Fe). However, carbonation efficiency is inhibited at pH under 7. Thus, to maximize carbonates production, pH

* Corresponding author at: National Institute for Space Research (INPE) Combustion and Propulsion Associated Laboratory (LCP) Rodovia Presidente Dutra, km 40, Cachoeira Paulista, SP, CEP 12630-000, Brazil.
E-mail addresses: gretta@lcp.inpe.br, grettagaf@yahoo.es (G.L.A. Arce Ferrufino).

https://doi.org/10.1016/j.jcou.2018.01.001
Received 7 May 2017; Received in revised form 27 November 2017; Accepted 2 January 2018
Available online 05 January 2018
2212-9820/

must be increased to levels above 9 [14–16]. Therefore, use of several acids and bases was thoroughly investigated in order to guarantee carbonates formation. Currently the main acid/base systems employed are HCl/NaOH and NH_4HSO_4/NH_4OH [9,12,17–19].

The advantage of the HCl/NaOH system is the recognized high efficiency of leaching stage when used hydrochloric acid (HCl), with a short reaction time of around 2 h [29,20] and a maximum of 30 min on carbonation stage to form carbonates when sodium hydroxide (NaOH) is used [16]. However, the main disadvantage related to this system is a high energy consumption to recover these chemical reagents when electrolytic process is used (3 MW h/tCO_2). Recently, Yuen et al. [13] indicated that energy consumption from this system could be reduced by 1.2 MW h/tCO_2 if bipolar membrane electrodialysis (BMED) is employed to recover HCl and NaOH as solutions. However, as mentioned by Bu et al. [21], their concentrations would be limited to 1 mol L^{-1}.

The main advantage in the case of the NH_4HSO_4/NH_4OH system is the possibility to broadly employ recovered chemical reagents. Moreover, previous CO_2 capture stages would not be necessary [22]. However, this system presents two disadvantages which limit its use: (i) a long reaction time of leaching of around 3 h; and (ii) high energy consumption to recover NH_4HSO_4 and NH_4OH from an aqueous solution of ammonium sulfate $(NH_4)_2SO_4$. Since low concentrations of NH_4HSO_4 solution is employed for leaching stage, large amounts of water are required, and hence, there is a considerable increase of energy consumption on following stages associated to $(NH_4)_2SO_4$ solution concentration processes [18].

Analysis of cost sensitivity indicate that if reaction time is reduced to 1 h, there is a possibility to reduce the capital cost by 50%, since the number and/or size of equipment can be reduced by half [13,22]. Thus, use of HCl would present advantages when compared to NH_4HSO_4.

On the other hand, several carbonates present different morphologies and their formation depends on temperature, pressure, and pH of the reaction medium [10,14,16,23–28]. CO_2 solubility in water is inhibited with an increase of temperature; however, formation of stable carbonates is favored when carbonation temperature is between 70 °C and 100 °C. Moreover, when solution pH is kept at values above 9, carbonate formation is also favored. Thus, for pH-swing mineral carbonation, strong bases (NaOH) as well as weak bases (NH_4OH) were employed. According to studies performed by Teir et al. [16]. Zhang et al. [28], both types of bases do not present advantages or disadvantages between them, with regards to keeping the solution pH. However, strong bases are more chemically stable than weak bases. Thus weak bases normally have a smaller dissociation degree which would allow an easy and fast recovery in stage following carbonation, when compared to a strong base.

Although several acid/base systems have been broadly studied by the aforementioned authors, the feasibility of a pH-swing mineral carbonation process based on a strong acid and a weak base (HCl/NH_4OH) was not yet elucidated. According to Zhang et al. [28], solutions prepared with 1.41 mol L^{-1} magnesium chloride ($MgCl_2$) might precipitate carbonates by using $CO_2/NH_3.H_2O$ in elevated pressures and moderate temperatures. A maximum carbonation efficiency of 73.6% was reported for a temperature of 100 °C and pressure of 6 MPa. However, it must be highlighted that carbonation efficiency was not yet investigated in atmospheric pressures.

This study proposes to evaluate the feasibility of a pH-swing mineral carbonation process based on HCl/NH_4OH system at atmospheric pressure and moderate temperatures. In order to accomplish this, an iron-rich mining waste from asbestos production process was used. The study investigates the silica production, selective precipitation of iron oxides, and carbonates production, as well as, the CO_2 capture efficiency.

2. Materials and methods

2.1. Materials

A mining waste was employed in this study, which came from the Minaçu Mine, located in Cana Brava, Goiás State, Brazil. The mining waste was named S-GO. It was crushed and grinded in order to obtain 150 µm particle size. This particle size range reports an acceptable energy requirement of 11 kW h by ton of processed mineral, in the previous stages of crushing and grinding [16,22,29,30]. Thus, the particle size classification in this study was done by using a number of sieves ASTM 120–80.

2.2. Characterization methods

Samples of each material (S-GO, S_1, S_2, S_3, L_1, L_2, L_3) were prepared and underwent the following analyses: thermogravimetric analysis (TGA); X-ray diffraction (XRD); wavelength dispersion sequential fluorescence (XRF); and inductively coupled plasma optical emission spectroscopy (ICP-OES).

Thermogravimetric analyses (TGA) were carried out to assess the materials thermal behavior. These TGA were carried out in a TA Instrument SDT TGA-DSC Q600 simultaneous system. Sample mass was approximately 30 ± 2 mg and a 90 µL alumina crucible was used for all tests, with a dynamic nitrogen atmosphere as purge gas, at a flow rate of 100 mL/min and a heating rate of 10 °C/min. The temperature range for S-GO and S1 were 30 °C − 1000 °C; for S4 and L3 were between 30 °C − 600 °C; and 30 °C − 300 °C, respectively.

Mineralogical composition of the materials was determined using a PANalytical X'pert3 Powder model X-ray diffraction analyzer (XRD). This device uses Cu Kα radiation in a range of 6–90° 2θ. Diffractograms obtained were processed using the HighScore Plus software. A mass of 1 ± 0.5 g was used for this analysis.

Sequential fluorescence with wavelength dispersion (XRF) was used for the quantitative analyses of materials chemical composition (SiO_2, MgO, CaO, Fe_2O_{3t}, K_2O, Na_2O, Al_2O_3, TiO_2, MnO, Cr_2O_3). It was carried out using a PANalytical Axios MAX-Advanced model device, with 4.0 kW operating power and 60 kV agitation. This device was employed to carry out a quantitative elemental chemical analysis of boron (B) and uranium (U). For such analysis, a 1 g mass sample was used for each material. ICP-OES analyses were conducted for determining the materials elemental composition(Si, Mg, Ca, Fe, K, Na, Al, Ti, Mn, Cr) with an Arcos Spectro model, inductively coupled with a plasma optical emission spectroscope.

2.3. Process description

A scheme of the process and its main reactions are presented on Fig. 1 and Table 1, respectively. The proposed process has four stages: 1) leaching, 2) purification, 3) carbonation, and 4) recovery of chemical reagents.

Leaching stage extracts reactive elements (Mg, Fe) from the mining wastes (S-GO) employing HCl solutions, in which the main involved reaction is described as R1 and presented on Table 1. This stage generates a leached solution (L_1) with high chloride concentrations from those reactive elements, as well as a solid residue (S_1) with elevated silica content [29,20].

The leached L_1 solution is conducted to the purification stage, in which a NH_4OH solution is employed for pH adjustment [27,30]. pH is increased during purification in order to precipitate Fe^{3+} and Fe^{2+} in the form of hydroxides, as shown on reactions R2 and R3 (Table 1). Formed hydroxides in this stage (S_2 and S_3) are separated from the resulting purified solution (L_2). Once Fe_t is separated, the purified L_2 solution presents high $MgCl_2$ concentration.

The purified L_2 solution is forwarded to the carbonation stage, in which it is mixed with an additional NH_4OH solution and CO_2,

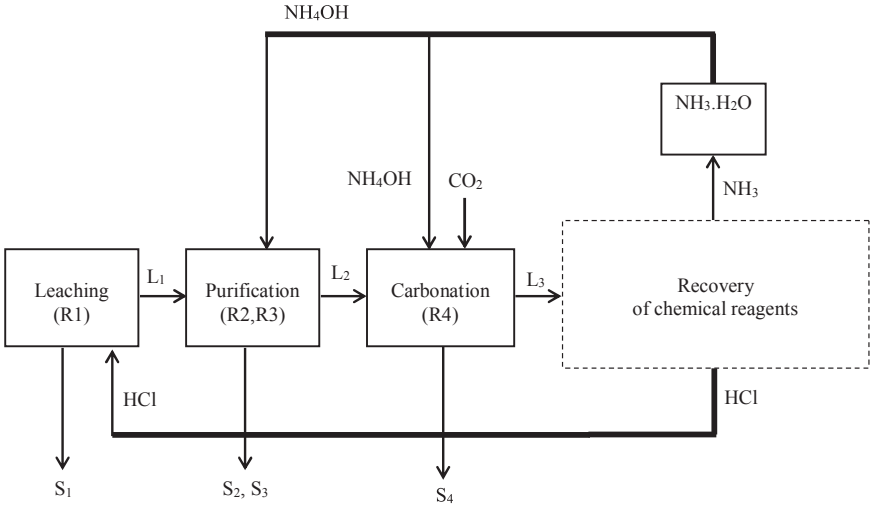

Fig. 1. Process scheme with several stages to pH-swing mineral carbonation based on HCl- NH_4OH system.

producing carbonates (S_4) according to reaction R4 presented on Table 1.

Produced carbonate (S_4) is precipitated and separated from NH_4Cl (L_3) aqueous solution. This solution is then sent to the last stage (recovery of chemical reagents), in which NH_4Cl can be separated into NH_3 and HCl according Zhang's methodology [28].

2.3.1. Leaching experiments

Mass/volume ratio for the experimental tests in this work were 74 g/L and, 37 g/L for stoichiometric conditions (T2E) and non-stoichiometric (T2 – acid excess), respectively. Initially, 100 mL of a 2 mol L^{-1} HCl solution was inserted into the vessel reactor of 500 mL and heated until 100 °C. Once the acid solution was heated, S-GO powder was added to the vessel reactor, which was equipped with a Graham condenser in order to avoid HCl loss by evaporation, as well as a thermocouple for temperature control. The reactor was continuously agitated with a magnetic stirrer set at 600–700 rpm during 2 h.

After each leaching process experimental test (T), two products were obtained, one solid residue (S_1) and one leachate solution (L_1). The solid residue S_1 was separated from the leachate solution L_1 through vacuum filtration. Following each experiment, residues (S_1) were dried during 2 h at approximately 105 °C. XRD, XRF, and TGA analyses were then carried out. Leachate solutions (L_1) were analyzed through ICP-OES in order to obtain Mg, Fe, and Si concentrations. Mg, Fe, and Si extraction in the leachate solutions (L_1) were calculated based on their content within S-GO, as showed in the Equation below (1):

$$X_i^L = \frac{V_{SOL} \times C_i}{M_{S-GO} \times i\%_{S-GO}} \times 100 \quad (1)$$

In which: X_i^L represents the leaching efficiency, $i\%_{S-GO}$ is the initial element content ("*i*": Mg, Fe, and Si) in the S-GO sample, $M_{S\text{-}GO}$ is the initial S-GO mass used in the experiments, and V_{SOL} is the leachate solution volume after 2 h of reaction. C_i is the concentration of elements in the leachate solution.

2.3.2. Impurities separation

Leachate solutions (L_1) were sent to the purification stage in order to separate the dissolved total iron (Fe_t). Separation was done in two steps, by controlled precipitation [9]. Thus, iron II (Fe^{2+}) and iron III (Fe^{3+}) were precipitated as hydroxides, when increased the solution pH. For this, a 30% w/w NH_4OH solution was employed. pH measurement was recorded through a METTLER TOLEDO pHmeter, *Seven Easy pHmeter S20,* with a ± 0.01 at 25 °C precision.

In the first purification step, NH_4OH addition was finalized when solution pH (pH_{P1}) reached a value of 5. Formation of a precipitate (S_2) was observed in this step, thus all Fe^{3+} was removed of aqueous solution as $Fe(OH)_3$ [9]. This precipitate was separated from the aqueous solution (or semi-purified – L'$_2$) by vacuum filtration. After that, the semi-purified L'$_2$ solution was sent to the second purification step in order to remove Fe^{2+}. Thus, an additional amount of NH_4OH in solution was added until L'$_2$ solution reached a pH value of 9 (pH_{P2}). Once the pH was adjusted, formation of another precipitate (S_3) was observed, which was separated from the purified solution (L_2) by vacuum filtration.

S_2 and S_3 solid precipitates were dried within an oven set at 105 °C during 12 h. They were then sent to elemental analysis to determine MgO, Fe_2O_{3t}, and SiO_2 through XRF. Purified L_2 solutions were sent for elemental analysis through ICP-OES in order to determine Mg, Fe, and Si concentrations. The calculation for purification efficiency was done by using Eq. (2) below:

$$X_i^P = \frac{[m_i^L - m_i^P]}{m_i^{S-GO}} \times 100, \quad (2)$$

In which: X_i^P, is the efficiency of the purification stage; *i*, is the Mg and Fe ions; m_i^L, is the concentration of each *i* in the leachate solution; m_i^P, is the concentration of each *i* in the purified L_2 solution.

2.3.3. Formation of carbonates

An alkaline pH is one determining factor to precipitate carbonates [14,16,27,28]. Thus, in the L_2 purified solutions, an NH_4OH solution was added at Mg:NH_4OH mass proportion of 1:2.9. This addition was

Table 1
Chemical reaction and thermodynamic properties from different process stages.

R.Q.	Reaction Equations	T °C	ΔH kJ	ΔG kJ
R1	$(Mg,Fe)_3(Si,Fe)_2O_5(OH)_4$ + **6HCl** = 3(Mg,Fe)Cl_2 + 2$FeCl_3$ + 2SiO_2 + 5H_2O	100	−321.3	−243
R2	$FeCl_2$ + 2NH_4OH = $Fe(OH)_2$ + 2**NH_4Cl**	25	−120.6	−97
R3	$FeCl_3$ + 3NH_4OH = $Fe(OH)_3$ + 3**NH_4Cl**	25	−101.2	−180
R4	5$MgCl_2$ + 10NH_4OH + 4CO_2 = $Mg_5(OH)_2(CO_3)_4$*4H_2O + 10**NH_4Cl**	90	−42.9	−98

done at room temperature (25 °C) and mixed at 400 rpm, guaranteeing a pH equivalent to 11.

Once NH_4OH was added to the L_2 purified solutions, the mixtures were conducted to the carbonation stage, in which the process temperature was set at 90 °C. However, before carbonation, the mixture was pre-heated to 60 °C, followed by CO_2 injection at a flow rate of 20 mL/min, until reaching 90 °C. CO_2 injection was kept for 60 min in order to guarantee total carbonates precipitation.

The reactor was equipped with a Graham condenser to avoid losses by NH_4OH evaporation. Besides this, a temperature and pH sensor was coupled to the reactor in order to have control of such variables during reaction. During 60 min of carbonation, a precipitate (S_4) was formed, which was separated from the liquid phase by vacuum filtration (carbonated solution – L_3).

The S_4 precipitates were dried in one oven at 105 °C during 12 h. Later on, the precipitates were characterized by XRF, XRD and TGA, respectively. On the other hand, the L_3 solutions were analyzed by ICP-OES to determine Mg concentration. Carbonation and CO_2 capture efficiency calculations were obtained using Eqs. (3) and (4), respectively.

$$X_{Mg}^{C} = \frac{(m_{Mg}^{I} - m_{Mg}^{C})}{m_{Mg}^{S-GO}} \times 100 \quad (3)$$

$$X_{CO_2}^{C} = \frac{(m_{CO_2}^{In} - m_{CO_2 i}^{C})}{m_{CO_2}^{In}} \times 100 \quad (4)$$

In which: X_{Mg}^{C}, is the carbonation efficiency; m_{Mg}^{I}, is the Mg mass in the L_2 purified solution; X_{Mg}^{C}, is the Mg mass in the L_3 solution after the carbonation stage; m_{Mg}^{S-GO}, is the Mg mass in the S-GO. On the other hand, $X_{CO_2}^{C}$, is the CO_2 capture efficiency, $m_{CO_2}^{In}$ is the CO_2 injected mass within the reactor; $m_{CO_2 i}^{C}$, the fixed CO_2 mass in the carbonate. The fixed CO_2 mass within the carbonate was quantified by TGA.

3. Results and discussion

3.1. Materials characterization

As it can be observed on Fig. 2, the S-GO mining waste presents a heterogeneous composition, with lizardite 1T as main mineral and secondary phases as brucite, magnesite, clinochrysotile and magnetite. According Arce et al. [2], this mineralogical characterization exhibits presence of clinochrysotile traces in the S-GO structure, indicating it as a hazardous waste. Rietveld quantification from different mineral phases resulted in 92% serpentines, 6.3% brucite, 1.09% magnesite, and 1.96% magnetite. Table 2 presents the S-GO chemical composition determined by XRF, which showed 43.33% MgO, 40.64% SiO_2, and 12.61% Fe_3O_4. Other metals were also detected by ICP-OES, such as K, Na, Al, Ti, Mn, and Cr in less than 2.4% of the solid. The BET area corresponding to S-GO was determined to be 6.7 cm^3/g.

Table 2
Chemical composition of S-GO mining waste.

XRF		ICP	
Oxides	Concentration (%)	Elements	Concentration (%)
SiO_2	40.64	Si	8.40
MgO	43.33	Mg	23.01
CaO	0.10	Ca	279.5[a]
Fe_2O_{3t}	12.61	Fe	4.49
K_2O	n.d.	K	< 0.01[a]
Na_2O	n.d.	Na	< 0.02[a]
Al_2O_3	1.17	Al	0.35
TiO_2	n.d.	Ti	140.3[a]
MnO	0.20	Mn	n.d.
Cr_2O_3	1.02	Cr	n.d.

n.d. = not detected.
[a] mg/kg.

Fig. 3 shows TG/DTG curves for S-GO, which exhibits a total loss of mass around 15.5% between 30 °C and 1000 °C. Three decomposition events were observed which corresponded to mineral phases in the S-GO. DTG peaks at 382 °C correspond to brucite and magnesite dehydroxylation, and DTG peaks at 600 °C and 659 °C correspond to lizardite 1T and clinochrysotile dehydroxylation, respectively [2].

As stated in Arce et al. [231]., the S-GO is derived from hydration of dunites (or olivine - $(Mg,Fe)_2SiO_4$), consequently there were brucite production along with serpentines. The phase diagram of the MgO-SiO_2-H_2O-FeO system can represent the serpentinization processes [12]. Besides that, depending on the P (atm) and T (°C), a minerals mixture (i.e. serpentines [serp - $Mg_3Si_2O_5(OH)_4$] + brucites [Brc – $Mg(OH)_2$] + magnetites [Mag – Fe_3O_4]) can be produced. Evans [32] suggested that the iron (Fe) – derived of the olivine ($(Mg,Fe)_2SiO_4$), that it is not embedded into of the serpentine structure by the cationic replacement mechanism, could be precipitated as Fe_3O_4. In addition, in high SiO_2 activities, Fe_3O_4 is not stable and the growth of Fe-rich serpentines is favored [32]. Moreover, Hostetler et al. [33] indicated that Fe inside brucite structure is related to exchange potential ($\mu\Delta(Fe^{2+}Mg_{-1})$). The $\mu\Delta(Fe^{2+}Mg_{-1})$ exerts a control on the molar fraction of Fe^{2+} turning it a ferromagnesium minerals [32]. So, the brucite contained within S-GO had a replacement of Fe^{2+} by Mg^{2+} from iron rich olivine.

There are structural differences between the serpentines; unlike the curve structures from chrysotile and antigorite, the lizardite have flat structures [34]. In the lizardite, the distance between flat layers is produced by cations replacement mechanism [35]. When the replacement of Si^{4+} by Al^{3+} in the tetrahedral sheets is realized, the forces of attraction between layers will become stronger [34]. Lizardite 1T has a flat structure that is more organized when compared with other polytypes, due to the affinity of lizardite 1T to replace Al^{3+} in the Si^{4+}

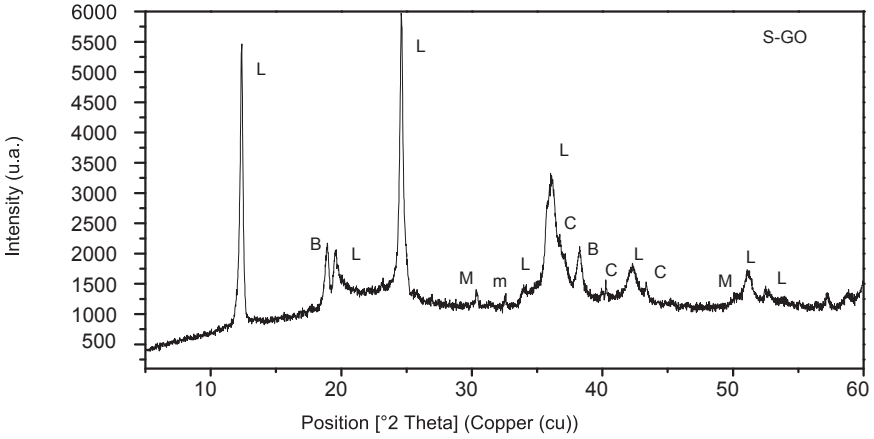

Fig. 2. S-GO X-ray diffractogram.

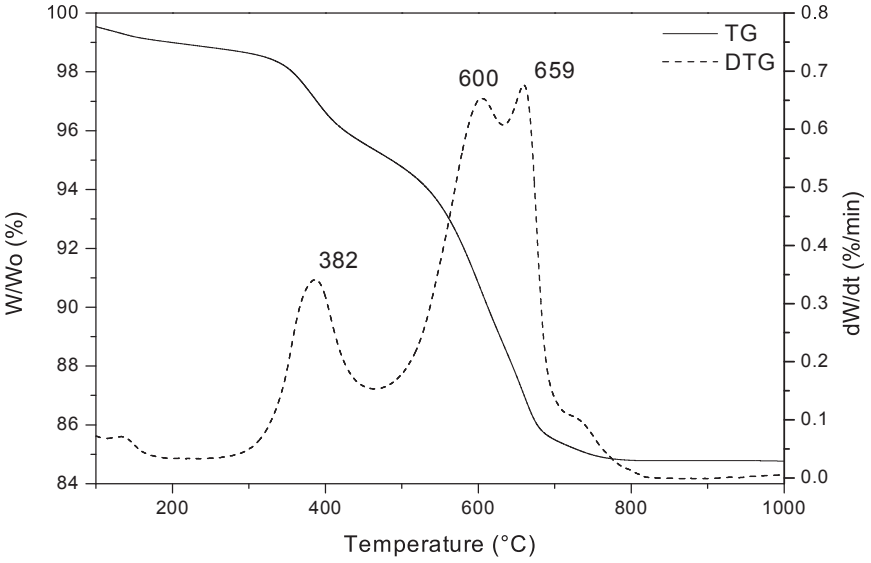

Fig. 3. TG/DTG curves from S-GO.

tetrahedral sheets. Therefore this affinity makes it less porous, and more stable [34,36]. Arce et al [2] suggested that lizardite 1T with Al_2O_3 content between 0.23–1.00% has less thermal and chemical stability. On the other hand, according to Lacinska et al. [37]. and Chamley [38], the lizardite stability can be affected by the Fe^{3+} replacement into Mg^{2+} octahedral and/or Si^{4+} tetrahedral sheets, however, the Fe^{3+} replacements into Mg^{2+} octahedral sheets could produce less stability [38]. According to Wicks and Wittacher [34], Fe^{2+} inside of the lizardite structure is unlikely since the atomic radius of Fe^{2+} would not allow the flat layer formation. So, crystalline structure of lizardite 1T presents higher iron content, mainly as Fe^{3+} and a low Al^{3+} content.

3.2. Leaching experiments

L_1 leachate solutions of both experimental tests, stoichiometric conditions (T2E) and acid excess (T2) were observed to be yellow; and solid residues (S_1) were slightly gray. Total mass of Mg, Fe and Si contained in L_1 leachate solutions, as well as, the efficiencies of Mg and Fe extraction from leaching stage are presented on Table 3, for both T2E and T2 tests. It can be observed that for both conditions, a high extraction efficiency were achieved using this type of mining waste, with an average values of 94 ± 2.0% for Mg and 95 ± 2.5% for Fe, respectively.

Although L_1 leachate solutions presented a higher amount of Mg than Fe, the amount of Fe extracted in T2E and T2 tests is significant when compared to other studies reported in the literature [20,39]. The S-GO behavior in the leaching stage can be attributed to the low content of Al^{3+}, once this reduces the thermal and chemical stability from this serpentinite [2,40,41].

It must be mentioned that the pH of the L_1 leached solutions (pH_L) were kept very acidic, even after 2 h of reaction, as 0.45 for T2E test and 0.02 for T2 test (Table 4). For pH-swing mineral carbonation, the pH is inversely proportional to leaching efficiency. As reported by McCutcheon et al. [15]; pHs higher than 1 can reduce the Mg extraction from serpentines.

On the other hand, direct mineral carbonation indicates that high Fe^{3+} content in Mg-bearing silicates which are also present in mining wastes, inhibits the formation of carbonates due to medium acidification [14,25,42].

In this study, Fe^{3+} present within S-GO is leached as ferric chloride ($FeCl_3$). The ferric chloride ($FeCl_3$) has promising catalytic abilities, then, it has been used as an acid catalyst in many processes [43,44]. The aqueous $FeCl_3$ solutions have the property to acidify the reactional medium, due to hydrolysis processes, since contact between $FeCl_3$ and H_2O favors H^+ release. Therefore, $FeCl_3$ had a catalytic effect in the leaching stage, promoting dissolution of other reactive metals, such as Mg. It should be highlighted that probably part of Fe^{2+} has been oxidized to Fe^{3+}, once the reaction was not realized in an inert atmosphere (N_2 not added into the reactor). In addition, although not investigated here in detail, the kinetics studies considering the structural modification (i.e the crystal order, the surface area and the porosity) of the iron-

Table 3
The amounts of metals in the solutions and the efficiency obtained from several stages of the process.

Stage	*Test*	*Solutions*		*Metal Mass*			*Efficiency*	
		Name	*V (mL)*	*Mg (mg)*	*Fe (mg)*	*Si (mg)*	*Mg (%)*	*Fe (%)*
S-GO	T2E	S-GO	100	1734[a]	357[a]	1000[a]	—	—
	T2	S-GO	100	891[a]	181[a]	507[a]		
Leaching	T2E	L1	90	1672	331	17	96.4	92.7
	T2	L1	88	826	177	13	92.7	97.7
Purification	T2E	L2	97	1475	10	12	11.4	89.9
	T2	L2	110	685	8	14	15.8	93.4
Carbonation	T2E	L3	115	5	10	12	84.8[b]	81[c]
	T2	L3	119	4	8	13	76.4[b]	42[c]

[a] Mass of Mg, Fe, and Si, within S-GO mining waste.
[b] carbonation efficiency.
[c] CO_2 capture efficiency.

Table 4
The volume of NH_4OH added and pH adjustment for each stage from the pH-swing mineral carbonation.

test		*Leaching*	*Purification*		*Carbonation*	
			P_1	P_2	*initial*	*Final*
T2E	NH_4OH added (mL)	0.00	4.6	2.4	18.1	0.00
	pH	0.45	5.04	9.00	10.85	8.85
T2	NH_4OH added (mL)	0.00	8.7	12.8	8.9	0.00
	pH	0.02	5.05	8.99	11.97	7.03

rich mining wastes should be carried out in future studies, since this will allow knowing the impact of $FeCl_3$ on the linkages of octahedral and tetrahedral sheets.

In Figs. 4a, b, 5a and b , a large structural S-GO modification can be observed after leaching on diffractograms and TG/DTG curves of the S_1 solid residues for both experimental tests (T2E and T2). Fig. 4a and b show curved patterns for S_1 diffractograms obtained on experimental tests T2E and T2, respectively. S-GO crystalline structure was modified to amorphous SiO_2, however, there was also the presence of crystalline silica mainly in the T2E stoichiometric test.

It must be emphasized that although high Mg and Fe extraction were achieved in this stage, S_1 solid residues diffractograms still indicate the presence of lizardite 1T, clinochrysotile, and brucite. This is corroborated by TG/DTG curves of S_1 solid residues presented on Fig. 5a, b, e, which show DTG decomposition peaks referring to such minerals (382 °C for brucite, 600 °C for lizardite 1T, and 659 °C for clinochrysotile). Nevertheless, although that a high leaching efficiency has been obtained, the total S-GO dissolution was not reached due to the Al_2O_3 content into the rock, which is above 1.00%.

On the Table 5, it is observed that the chemical composition of S_1 solid residues obtained in both T2E and T2 tests, exhibits a content of MgO, Fe_2O_{3t}, and SiO_2, approximately of 3.6–2.8%, 2.3–2.0% and 90.4–91.5%, respectively. Such S_1 residues are not yet appropriate to be commercialized, since silica purity must be higher than 99% [6]. However, SiO_2 content could be increased by using purification processes.

3.3. Impurities separation

Once the leaching stage was concluded, L_1 solutions were sent for pH adjustment until approximately 5 and 9, in order to perform selective precipitation of Fe^{3+} and Fe^{2+}. Table 4 shows total volumes of NH_4OH added to adjust pH (P_1 and P_2) in the purification stage. It can be observed that NH_4OH added on T2 experimental test is three times higher than T2E experimental test. Large base consumption for pH adjustment during the T2 experimental test is due to excess acid used during the leaching stage, which was twice the stoichiometric value. It must be mentioned that the acid excess only increased Mg and Fe extraction by 5%. Thus, by using materials with S-GO characteristics, a stoichiometric condition would reduce the consumption of chemical reagents.

Table 3 shows Mg, Fe and Si amounts within the L_2 purified solution, as well as precipitation efficiencies from the purification stage. It can be seen that an average of Fe precipitation efficiency of approximately 91.7 ± 1.9% was obtained for both T2E and T2 experimental tests, moreover, it was also observed an average of 13.6 ± 2.3% Mg precipitated in this stage.

On Table 5, in the purification stage can be observed a higher production (m_p) of S_2 precipitate than S_3 precipitate, indicating a high Fe^{3+} content, this is congruent with lizardite 1T inherent characteristic [34]. S_3 precipitate in small amount refers to ferrous brucite ([Mg,Fe$(OH)_2$]) and/or clinochrysotile [2,45]. The concentration of Fe_2O_{3t} in S_2 is of approximately 91.2% and 89.5% for experimental tests T2E and T2, respectively, and in the S_3 precipitate is of approximately 90.7% and 88.3% for tests T2E and T2, respectively (Table 5).

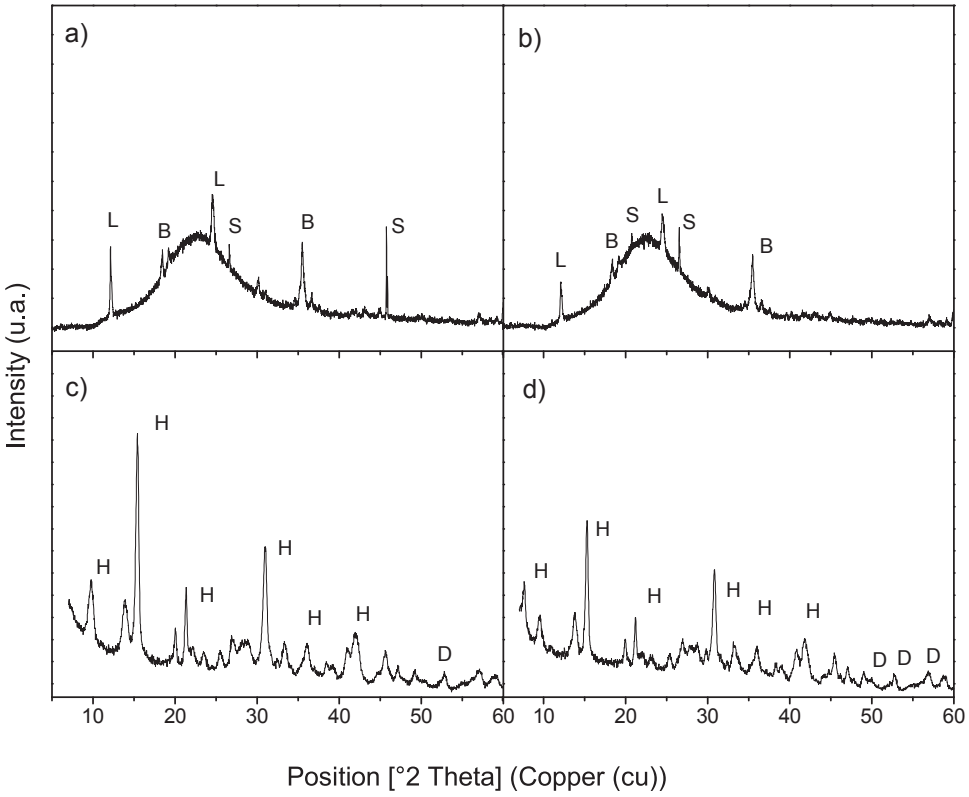

Fig. 4. Diffractograms for solid residues. a) S_1 solid residue of T2E, b) S_1 solid residue of T2, c) S_4 solid residue of T2E and d) S_4 solid residue of T2.

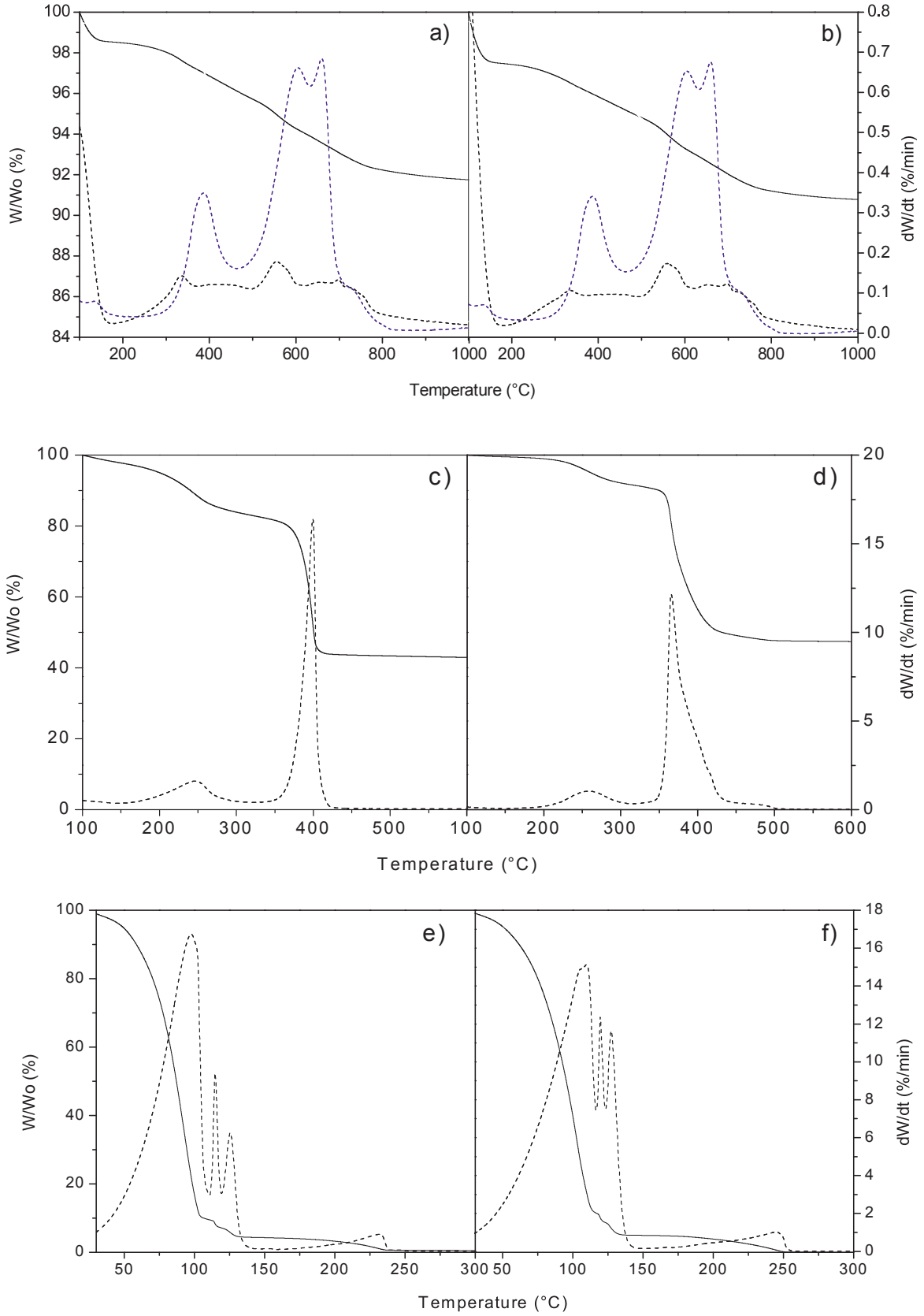

Fig. 5. TG curves (line) and DTG curves (dot lines) for residues obtained during several stages of the pH-swing mineral carbonation process. a) S_1solid residue of T2E b) S_1 solid residue of T2,c) S_4 solid residues of T2E, d) S_4 solid residues of T2, e)L_3 solutions of T2E and f) L_3 solution of T2.

Table 5
Mass of metals and efficiencies obtained in several stages of the pH-swing mineral carbonation process using HCl/NH_4OH.

Stage	*Test*	*Solid Products*		*Metal Concentration (%)*		
		Name	$m_{p\ (g)}$	*MgO*	Fe_2O_{3t}	SiO_2
S-GO	T2E	S-GO	7.4	43.33	12.61	40.64
	T2	S-GO	3.7	43.33	12.61	40.64
Leaching	T2E	S_1	2.8	3.6	2.3	**90.4**
	T2	S_1	1.5	2.8	2.0	**91.5**
Purification	T2E	S_2	0.73	2.4	**91.2**	1.3
		S_3	0.18	0.6	**90.7**	0.5
	T2	S_2	0.51	4.4	**89.5**	1.6
		S_3	0.01	1.2	**88.3**	0.3
Carbonation	T2E	S_4	4.53	**43.7**	0.013	0.5
	T2	S_4	2.1	**40.5**	0.007	0.1

3.4. Carbonates precipitation

As soon as the L_2 solutions were purified, they were sent to carbonation stage. In order to keep the alkaline pH of the L_2 solution, NH_4OH was added to both T2E and T2 experimental tests. Table 4 shows that the T2E test employed a larger amount of NH_4OH, due to a higher amount of Mg contained in the T2E stoichiometric test when compared to T2 tests with excess acid. The pH value after base addition was 11.41 ± 0.56 for both experimental tests.

After pH adjustment, the mixture (L_2 solution and NH_4OH) was preheated until 60 °C and then CO_2 was injected. When this procedure was performed, immediate carbonates formation and precipitation were observed, as well as a decrease of solution pH, by two and/or three units during the first 30 min of carbonation. A stable pH was obtained between 7 and 9, during a total reaction time equivalent to 60 min. So, Table 3 shows a carbonation efficiency of 84.8 and 76.4% for both T2E and T2 tests, respectively.

In pH-swing mineral carbonation, nesquehonite ($MgCO_3.3H_2O$) and hydromagnesite ($Mg_5(CO_3)_4(OH)_2.4H_2O$) are frequently sintered as carbonates [17,37,46]. According to Wilson et al. [46], to capture of CO_2, the best sintered carbonates must have a molar ratio of MgO to CO_2 equal to 1:1 (i.e. magnesite ($MgCO_3$), nesquehonite ($MgCO_3.3H_2O$) among others), however, their environmental stability is low. On the other hand, although the carbonates with molar ratio equal to 5:4 (i.e. hydromagnesite ($Mg_5(CO_3)_4(OH)_2.4H_2O$), dypingite (($Mg_5(CO_3)_4(OH)_2.5H_2O$)) do not capture as much CO_2 as carbonates with molar ratio 1:1, their environmental stability is better [46]. Therefore, carbonates precipitation depend on both the environmental stability and the CO_2 capture efficiency.

In this study can be seen that the carbonates obtained in T2E and T2 experimental tests (S_4) have a MgO content of 43.7% and 40.5%, respectively (Table 5). Figs. 4c, d, 5c and d show X-ray diffractograms and TG/DTG curves for carbonates obtained after the carbonation stage (S_4). Narrow peaks were observed on S_4 precipitate diffractograms (Fig. 4c and d) which reflect a high crystallinity of carbonates. Mineralogical analysis of S_4 precipitates obtained from T2E test (Fig. 4c) indicated that the main phase is hydromagnesite, however, there are traces of dypingite.

According to Wilson et al. [46]., in direct mineral carbonation using mine waste, the hydrated carbonates with MgO:CO_2 molar ratio of 5:4 are formed from hydrated carbonates with MgO:CO_2 molar ratio of 1:1. Hence, the nesquehonite ($MgCO_3.3H_2O$) decomposition can produce dypingite ($Mg_5(CO_3)_4(OH)_2.5H_2O$) and hydromagnesite ($Mg_5(CO_3)_4(OH)_2.4H_2O$) [46]. Additionally Glasser et al. [8] indicated that the increase of dypingite and hydromagnesite from nesquehonite depends on the quantities of H_2O and CO_2 in the reaction. Studies related to pH-swing mineral carbonation indicated that dypingite can be produced when initial temperature of carbonation is about 60 °C [27].

In this study was produces dypingite, due to carbonates precipitation started at 60 °C [27]. On the other hand, the S_4 precipitate diffractogram obtained from T2 test (Fig. 5d) has a higher dypingite content, probably due to excess H_2O and CO_2 in the reaction medium [8,47]. When TG/DTG curves from Fig. 5c and d are observed, it can be noticed that the carbonate from T2E test has a higher purity than the carbonate from T2 test, thus confirming the XRD patterns (Fig. 4c and d).

From the carbonates mass loss (S_4) were observed on TG curves, it can be noticed that the carbonate obtained in T2E test presents approximately 36.7% of CO_2 fixed as CO_3^{2-}. However, the carbonate obtained in T2 presents 44.1% of CO_2 fixed. Thus, the T2E condition was able to form carbonates with a CO_2 capture efficiency of 81%, which is twice more captured CO_2 when compared to T2 test condition (Table 3).

Since the best CO_2 capture efficiency was obtained for the T2E test, a mass balance was done for the whole process. Results are presented on Table 6. The calculation basis employed for this study was the capture of 1 ton of CO_2. Calculations indicate that 4 ton of S-GO mineral waste will be employed for each ton of captured CO_2, as well as 2.6 ton of HCl, and 4.5 ton of NH_4OH. However, 1.7 ton of SiO_2, 0.55 ton of iron oxide, and 2.7 ton of hydromagnesite could be produced. It must be mentioned that this process could be optimized to reduce consumption of chemical reagents.

On the other hand, recovery of chemical reagent (HCl and NH_4OH) could be realized by Zhang's methodology [28]. However, it must be mentioned that, in this experimental study, after the carbonation process, the L_3 solution was cooled to room temperature (25 °C). In this temperature was observed the formation of crystals in the L_3 aqueous solution, indicating NH_4Cl supersaturation. These L_3 solutions were characterized by TGA. Fig. 5e and f show L_3 solutions thermal decomposition for experimental tests T2E and T2, respectively. Total decomposition of the L_3 aqueous solution was observed up to 250 °C. The first thermal decomposition event from the DTG curve refers to water evaporation. In this region, a mass loss is observed around 80% and 86%, for T2E and T2 tests, respectively. After water elimination, the DTG curve presents three peaks due to salt decomposition, indicating different events, which can be related to decomposition of NH_4Cl in NH_3 and HCl.

Although this study demonstrated the feasibility to produce silica, iron oxide and carbonates with high purity in atmospheric pressure and moderate temperature using pH-swing mineral carbonation based on HCl/NH_4OH system, there is evidently a need for further investigations about the recovery of chemical reagent (i.e. HCl and NH_4OH) aiming a low energy consumption.

This type of HCl/NH_4OH system could make the pH-swing mineral carbonation process more efficient, since it can employ higher HCl concentrations. An increase of HCl concentration intensifies the extraction of reactive elements, generating a silica with high degree of purity [26]. Increasing acid concentration can also reduce water consumption, which is a critical point for the pH-swing mineral carbonation process, due to environmental limitations [13].

Table 6
NH_4OH added into aqueous solution for precipitation of the products.

CO_{2SEQ} ton	S-GO ton	HCl ton	NH_4OH ton	SiO_2 ton	Fe ton	Hydro-Mg ton	CO_{2CAP} %
1	4.0	2.6	4.5	1.7	0.55	2.7	81

4. Conclusion

This study evaluated the feasibility to produce silica, iron oxide and carbonates with high purity using one HCl/NH_4OH system for pH-swing mineral carbonation, at atmospheric pressure and moderate temperatures (90 °C). Besides this, the possibility to recover chemical reagents was explored through NH_4Cl thermal decomposition, which is formed after the carbonation stage.

Results indicated that the S-GO mining waste was appropriate to be employed in pH-swing mineral carbonation, even though it presented lizardite 1T as the main phase. The Fe^{3+} content in S-GO acted as a catalyst, aiding the leaching of other reactive metals, since it generated a strong acidic medium during the reaction process. This is due to $FeCl_3$ hydrolysis in aqueous solutions, causing an intrinsic HCl regeneration.

High Mg and Fe extraction efficiency was achieved in the first process stage (95 ± 2%), even in stoichiometric conditions. The solid residue obtained after the leaching stage (S_1) was mainly silica (SiO_2) with 90% purity content. Such silica purity can be improved if HCl concentrations higher to 2 mol L^{-1} were employed.

Use of stoichiometric conditions (T2E) during the purification stage reduces the volume of NH_4OH solution employed, by approximately three folds, when compared to acid excess conditions (T2). Efficiency of the purification stage was high, with iron removal of around 91.7 ± 1.9%. However, a loss of Mg was detected during this step, of approximately 13.6 ± 2.3%.

Hydromagnesite was formed during the carbonation stage, which had a 80.6 ± 3.5% efficiency. 81% of the total CO_2 injected was fixed by hydromagnesite inside the reactor, through crystallographic capture. This study showed a good yield of silica, iron oxides, and carbonates production. Besides this, the recovery study for chemical reagents indicated that NH_4Cl crystallization temperature would favor its regeneration into NH_3 and HCl, which can be conducted at temperatures below 250 °C.

Acknowledgements

The authors are thankful to FAPESP for post-doctorate project number 2013/21244-5 and as well as CNPq for project number 150868/2017-0, which supported this study. In addition, they acknowledge the company that provided study materials: Mineração Associada (SAMA S.A.).

References

[1] G. Gadikota, C. Natali, C. Boschi, A.-H.A. Park, Morphological changes during enhanced carbonation of asbestos containing material and its comparison to magnesium silicate minerals, J. Hazard. Mater. 264 (2014) 42–52, http://dx.doi.org/10.1016/j.jhazmat.2013.09.068.

[2] G.L.A.F. Arce, T.G. Soares Neto, I. Ávila, C.M.R. Luna, J.A. Carvalho Jr., Leaching optimization of mining wastes with lizardite and brucite contents for use in indirect mineral carbonation through the pH swing method, J. Clean. Prod. 141 (2017) 1324–1336, http://dx.doi.org/10.1016/j.jclepro.2016.09.204.

[3] A. Bloise, T. Critelli, M. Catalano, C. Apollaro, D. Miriello, A. Croce, et al., Asbestos and other fibrous minerals contained in the serpentinites of the Gimigliano-Mount Reventino Unit (Calabria, S-Italy), Environ. Earth Sci. 71 (2014) 3773–3786, http://dx.doi.org/10.1007/s12665-013-3035-2.

[4] J. Li, Q. Dong, K. Yu, L. Liu, Asbestos and asbestos waste management in the Asian-Pacific region: trends, challenges and solutions, J. Clean. Prod. 81 (2014), http://dx.doi.org/10.1016/j.jclepro.2014.06.022.

[5] A. Valouma, A. Verganelaki, P. Maravelaki-kalaitzaki, E. Gidarakos, Chrysotile asbestos detoxification with a combined treatment of oxalic acid and silicates producing amorphous silica and biomaterial, J. Hazard. Mater. 305 (2016) 164–170.

[6] A. Fedoročková, P. Raschman, G. Sučik, B. Plešingerová, Ľ. Popovič, J. Briančin, Processing of serpentinite tailings to pure amorphous silica, Ceramics 59 (2015) 275–282.

[7] S.N. Nam, S. Jeong, H. Lim, Thermochemical destruction of asbestos-containing roofing slate and the feasibility of using recycled waste sulfuric acid, J. Hazard. Mater. 265 (2014) 151–157, http://dx.doi.org/10.1016/j.jhazmat.2013.11.004.

[8] F.P. Glasser, G. Jauffret, J. Morrison, J.-L. Galvez-Martos, N. Patterson, M.S.-E. Imbabi, Sequestering CO2 by mineralization into useful nesquehonite-based products, Front. Energy Res. 4 (2016) 1–7, http://dx.doi.org/10.3389/fenrg.2016.00003.

[9] A. Hemmati, J. Shayegan, J. Bu, T.Y. Yeo, P. Sharratt, Process optimization for mineral carbonation in aqueous phase, Int. J. Min. Process. 130 (2014) 20–27, http://dx.doi.org/10.1016/j.minpro.2014.05.007.

[10] A. Sanna, M. Uibu, G. Caramanna, R. Kuusik, M.M. Maroto-Valer, A review of mineral carbonation technologies to sequester CO2, Chem. Soc. Rev. 43 (2014) 8049–8080, http://dx.doi.org/10.1039/C4CS00035H.

[11] J. Sipilä, S. Teir, R. Zevenhoven, Carbon Dioxide Sequestration by Mineral Carbonation - Literature Review Update 2005–2007, Espoo, Finland, (2008) (accessed September 16, 2013), http://users.abo.fi/rzevenho/MineralCarbonationLiteratureReview05-07.pdf.

[12] X. Wang, M.M. Maroto-Valer, Dissolution of serpentine using recyclable ammonium salts for CO2 mineral carbonation, Fuel 90 (2011) 1229–1237, http://dx.doi.org/10.1016/j.fuel.2010.10.040.

[13] Y.T. Yuen, P.N. Sharratt, B. Jie, Carbon dioxide mineralization process design and evaluation: concepts, case studies, and considerations, Environ. Sci. Pollut. Res. 23 (2016) 22309–22330, http://dx.doi.org/10.1007/s11356-016-6512-9.

[14] P. Córdoba, Q. Liu, S. Garcia, M. Maroto-Valer, Understanding the importance of iron speciation in oil-field brine pH for CO2 mineral sequestration, J. CO2 Util. 16 (2016) 78–85, http://dx.doi.org/10.1016/j.jcou.2016.06.004.

[15] J. McCutcheon, G.M. Dipple, S.A. Wilson, G. Southam, Production of magnesium-rich solutions by acid leaching of chrysotile: a precursor to field-scale deployment of microbially enabled carbonate mineral precipitation, Chem. Geol. 413 (2015) 119–131, http://dx.doi.org/10.1016/j.chemgeo.2015.08.023.

[16] S. Teir, R. Kuusik, C.-J. Fogelholm, R. Zevenhoven, Production of magnesium carbonates from serpentinite for long-term storage of CO2, Int. J. Min. Process. 85 (2007) 1–15, http://dx.doi.org/10.1016/j.minpro.2007.08.007.

[17] S. Teir, S. Eloneva, C. Fogelholm, R. Zevenhoven, Fixation of carbon dioxide by producing hydromagnesite from serpentinite, Appl. Energy 86 (2009) 214–218, http://dx.doi.org/10.1016/j.apenergy.2008.03.013.

[18] A. Sanna, J. Gaubert, M.M. Maroto-Valer, Alternative regeneration of chemicals employed in mineral carbonation towards technology cost reduction, Chem. Eng. J. 306 (2016) 1049–1057, http://dx.doi.org/10.1016/j.cej.2016.08.039.

[19] A. Azdarpour, M. Asadullah, E. Mohammadian, H. Hamidi, R. Junin, M.A. Karaei, A review on carbon dioxide mineral carbonation through pH-swing process, Chem. Eng. J. 279 (2015) 615–630, http://dx.doi.org/10.1016/j.cej.2015.05.064.

[20] S. Teir, H. Revitzer, S. Eloneva, C.-J. Fogelholm, R. Zevenhoven, Dissolution of natural serpentinite in mineral and organic acids, Int. J. Min. Process. 83 (2007) 36–46, http://dx.doi.org/10.1016/j.minpro.2007.04.001.

[21] J. Bu, P. Bai, P. Sharratt, Carbon Dioxide Capture With Regeneration of Salt: International Publication Number WO 2012/050530 A1, (2012).

[22] A. Sanna, X. Wang, A. Lacinska, M. Styles, T. Paulson, M.M. Maroto-Valer, Enhancing Mg extraction from lizardite-rich serpentine for CO2 mineral sequestration, Min. Eng. 49 (2013) 135–144, http://dx.doi.org/10.1016/j.mineng.2013.05.018.

[23] G. Gadikota, K.J. Fricker, S.-H. Jang, A.-H.A. Park, Carbonation of silicate minerals and industrial wastes and their potential use as sustainable construction materials, Carbon Dioxide Util Closing Carbon Cycle, 1st ed., (2015), pp. 115–137, http://dx.doi.org/10.1016/B978-0-444-62746-9.00008-6 American C, Washington DC.

[24] G. Gadikota, E.J. Swanson, H. Zhao, A.-H.A. Park, Experimental design and data analysis for accurate estimation of reaction kinetics and conversion for carbon mineralization, Ind Eng. Chem. Res. 53 (2014) 6664–6676, http://dx.doi.org/10.1021/ie500393h.

[25] G. Gadikota, J. Matter, P. Kelemen, A.-H.A. Park, Chemical and morphological changes during olivine carbonation for CO2 storage in the presence of NaCl and NaHCO3, Phys. Chem. Chem. Phys. 16 (2014) 4679–4693, http://dx.doi.org/10.1039/c3cp54903h.

[26] G. Gadikota, A.A. Park, Chapter 8 – accelerated carbonation of Ca- and Mg-bearing minerals and industrial wastes using CO2, in: P. Styring, Q. Elsje Alessandra, K. Armstrong (Eds.), Carbon Dioxide Util Closing Carbon Cycle, 1st ed., Elsevier, Amsterdam, 2015, pp. 115–130.

[27] A. Hemmati, J. Shayegan, P. Sharratt, T.Y. Yeo, J. Bu, Solid products characterization in a multi-step mineralization process, Chem. Eng. J. 252 (2014) 210–219, http://dx.doi.org/10.1016/j.cej.2014.04.112.

[28] J. Zhang, R. Zhang, H. Geerlings, J. Bi, Mg-silicate carbonation based on an HCl- and NH 3-recyclable process: effect of carbonation temperature, Chem. Eng. Technol. 35 (2012) 525–531, http://dx.doi.org/10.1002/ceat.201100425.

[29] A. Sanna, M. Dri, M.M. Maroto-Valer, Carbon dioxide capture and storage by pH swing aqueous mineralisation using a mixture of ammonium salts and antigorite source, Fuel. 114 (2013) 153–161, http://dx.doi.org/10.1016/j.fuel.2012.08.014.

[30] X. Wang, M.M. Maroto-Valer, Integration of CO2 capture and mineral carbonation by using recyclable ammonium salts, ChemSusChem 4 (2011) 1291–1300, http://dx.doi.org/10.1002/cssc.201000441.

[31] G.L.A.F. Arce, T.G.S. Neto, I. Ávila, C.M.R. Luna, J.C. dos Santos, J.A. Carvalho, Influence of physicochemical properties of Brazilian serpentinites on the leaching process for indirect CO2 mineral carbonation, Hydrometallurgy 169 (2017) 142–151, http://dx.doi.org/10.1016/j.hydromet.2017.01.003.

[32] B.W. Evans, Control of the products of serpentinization by the Fe2+ Mg-1 exchange potential of olivine and orthopyroxene, J. Petrol. 49 (2008) 1873–1887, http://dx.doi.org/10.1093/petrology/egn050.

[33] P.B. Hostetler, R.G. Coleman, F.A. Mumpton, Brucite in alpine Serpentinites, Am. Mineral. 51 (1966) 74–98, http://dx.doi.org/10.1163/_q3_SIM_00374.

[34] F.J. Wicks, E.J.W. Whittaker, A reappraisal of the structures of the serpentine minerals, Can. Mineral. 13 (1975) 227–243.

[35] R.B. Frost, J.S. Beard, On silica activity and serpentinization, J. Petrol. 48 (2007) 1351–1368, http://dx.doi.org/10.1093/petrology/egm021.

[36] C. Viti, M. Mellini, Contrasting chemical compositions in associated lizardite and

chrysotile in veins from Elba, Italy, Eur. J. Mineral. 9 (1997) 585–596 http://eurjmin.geoscienceworld.org/content/9/3/585.short.
[37] A. Sanna, A. Lacinska, M. Styles, M.M. Maroto-Valer, Silicate rock dissolution by ammonium bisulphate for pH swing mineral CO2 sequestration, Fuel Process. Technol. 120 (2014) 128–135, http://dx.doi.org/10.1016/j.fuproc.2013.12.012.
[38] H. Chamley, Clay Sedimentology, Springer, New York, 1989, http://dx.doi.org/10.1007/s13398-014-0173-7.2.
[39] A. Sanna, X. Wang, A. Lacinska, M. Styles, T. Paulson, M.M. Maroto-Valer, Enhancing Mg extraction from lizardite-rich serpentine for CO2 mineral sequestration, Min. Eng. 49 (2013) 135–144, http://dx.doi.org/10.1016/j.mineng.2013.05.018.
[40] A.M. Lacinska, M.T. Styles, K. Bateman, D. Wagner, M.R. Hall, C. Gowing, et al., Acid-dissolution of antigorite, chrysotile and lizardite for ex situ carbon capture and storage by mineralisation, Chem. Geol. 437 (2016) 153–169, http://dx.doi.org/10.1016/j.chemgeo.2016.05.015.
[41] C. Viti, Serpentine minerals discrimination by thermal analysis, Am. Mineral. 95 (2010) 631–638, http://dx.doi.org/10.2138/am.2010.3366.
[42] G.P. Assima, F. Larachi, J. Molson, G. Beaudoin, Comparative study of five Québec ultramafic mining residues for use in direct ambient carbon dioxide mineral sequestration, Chem. Eng. J. 245 (2014) 56–64, http://dx.doi.org/10.1016/j.cej.2014.02.010.
[43] I. Muthuvel, S. Dineshkumar, K. Thirumurthy, S. Rajasri, G. Thirunarayanan, A New Solid Acid Catalyst FeCl 3 / Bentonite for Aldol Condensation Under Solvent-Free Condition 55 (2016), pp. 252–260.
[44] Z. Wang, X. Sun, J. Wu, $FeCl_3$: An efficient catalyst for reactions of electron-rich arenes with imines or aziridines, Tetrahedron 64 (2008) 5013–5018, http://dx.doi.org/10.1016/j.tet.2008.03.081.
[45] H.C. Oskierski, B.Z. Dlugogorski, G. Jacobsen, Sequestration of atmospheric CO2 in a weathering-derived, serpentinite-hosted magnesite deposit: 14C tracing of carbon sources and age constraints for a refined genetic model, Geochim. Cosmochim. Acta 122 (2013) 226–246, http://dx.doi.org/10.1016/j.gca.2013.08.029.
[46] S.A. Wilson, G.M. Dipple, I.M. Power, J.M. Thom, R.G. Anderson, M. Raudsepp, et al., Carbon dioxide fixation within mine wastes of ultramafic-hosted ore deposits: examples from the Clinton Creek and Cassiar Chrysotile deposits, Can. Econ. Geol. 104 (2009) 95–112, http://dx.doi.org/10.2113/gsecongeo.104.1.95.
[47] I.M. Power, S.A. Wilson, G.M. Dipple, Serpentinite carbonation for CO2 sequestration, Elements 9 (2013) 115–121, http://dx.doi.org/10.2113/gselements.9.2.115.